NUMERICAL ANALYSIS AND STUDY ON LASER FILLED WIRE BRAZING OF CU-AL HETEROMETALS

Guang ZENG[1], Shaokai KANG[1], Yalong ZHANG[1], Qiang BIAN[2,*] , Quanwei LIU[1], Chunjiang ZHAO[2], Kun CHEN[1]

This article establishes a heat source model for laser wire filling brazing of copper aluminum heteroalloys using nonlinear transient heat conduction theory. On this basis, the finite element model of laser wire-filled brazing is constructed by Abaqus software, and the Python subroutine containing laser heat source parameters and walking path was called to complete the definition of life and death unit. Based on this model, the variation law and optimum range of laser power, brazing speed and spot diameter on joint temperature, penetration depth and penetration width were studied. Through research, it was found that the temperature field on both sides of copper and aluminum exhibits an asymmetric distribution, with the temperature on the copper side significantly higher than that on the aluminum side. With the increase of laser power, the highest temperature during welding increases, and the solder melts fully. Thus, too high power will lead to too wide weld and affect the quality of the joint. With the increase of speed, the highest temperature decreases, the spot diameter becomes smaller, and the width of molten pool became narrower. If the speed is too high, yet the quality of welded joints will be uneven. In order to ensure that the highest temperature of the welding area and the size of the heat affected zone are within the appropriate range, it is found that high-quality welded joints can be obtained by selecting laser power P=1100w and speed 0.04 m/s.

Keywords: Laser wire filling brazing; Heterogeneous alloy; Temperature field; Numerical analysis

1. Introduction

Laser wire-fill brazing is a process in which a small micro-area is heated by an ultra-high-energy laser beam on the connection part, causing the solder and base material to melt rapidly to form a micro-melting pool and complete the welding process [1-3]. Laser brazing with wire filler has the advantages of small deformation, small weld, low residual stress, high efficiency and good weld performance. And it can achieve the welding of multiple layers or heterogeneous metals with less heat input and heat zone influence [4-5].

[1] School of Aerospace Engineering, ZhengZhou University of Aeronautics, China, e-mail:zengg8899@163.com
[2] School of Mechanical Engineering, Taiyuan University of Science and Technology, China
* e-mail:B2021231026@stu.tyust.edu.cn (corresponding author)

Copper is widely used in aerospace, power transmission, electronic devices and other industrial fields due to its excellent thermal conductivity, electrical conductivity and processability. However, it is expensive and has limited reserves. And metallic aluminum has low price, large reserves and good corrosion resistance, electrical conductivity and thermal conductivity [6,7]. Generally speaking, when the component structure is working, only some parts need to bear large heat, medium and load. Therefore, copper and aluminum heterogeneous metals can be welded through joints to form aluminum/copper heterostructures. Under the condition of meeting the use function, the cost and weight are reduced, and the advantages of copper and aluminum can be brought into play respectively. Due to the low energy density of common arc welding and fusion welding methods, and the obvious differences in the melting point, thermal conductivity, linear expansion coefficient and other characteristic parameters of copper and aluminum, the heat input will be too large, and more hard and brittle phase compounds will appear at the copper-aluminum joint, which will affect the mechanical properties of the joint. Although brazing and pressure welding can obtain joints with good strength and quality, there are some problems such as high cost, low efficiency and large deformation [8,9]. Laser brazing with wire filler can overcome these shortcomings, realize high energy density, fast and micro-zone welding, and obtain high strength copper-aluminum joint quality.

Many scholars have studied the welding characteristics and process characteristics of copper-aluminum heterogeneous connection structure.

Wan et al. [10] used Zn-5%Al flux-cored wire to braze dissimilar metals of copper and aluminum by laser filler wire, and studied the morphology, microstructure, mechanical and energy characteristics of the joint. Dimatteo et al. [11] studied the influence of spot diameter in self-lap welding of copper and aluminum dissimilar laser, and found that smaller spot diameter is helpful to form a good weld bead and control the penetration depth better. Such as, Envelope [12] studied the influence of laser brazing process parameters on copper-aluminum dissimilar metal joints, and obtained the corresponding relationship between welding speed and microstructure. Huang et al. [13] studied the microstructure evolution characteristics of aluminum/copper joint with the aid of bypass coupling arc welding method. Jin et al. [14] used different annealing temperatures to treat the copper-aluminum joint after friction stir welding to study the growth mechanism and optimum temperature of intermetallic compound layer in lap joint. Darina [15] used electron beam to weld copper-aluminum alloy plates, and studied the influence of beam scanning geometry on the structure and mechanical properties of welded joints. These studies mainly study the microstructure, diffusion mechanism, morphology and mechanical properties of the joint interface through experiments. These research results have greatly promoted the development of copper-aluminum bonding technology and laser brazing process.

In the process of laser brazing, the selection of laser parameters and process parameters is very important to the quality of the joint. The experimental method not only has long period and high cost, but also some parameters (internal temperature of joint) can not be obtained by experimental method. Based on the nonlinear transient heat conduction theory, the numerical model of laser brazing of T2 copper and aluminum alloy 6063 is established by ABAQUS software. The effects of laser power, brazing speed and spot diameter on the temperature, penetration depth and width of joint area were studied, and the optimum range was determined. This study can provide a basis for the selection and optimization of laser brazing process parameters for heterogeneous metals.

2 Construction of a finite element model for laser wire-fill brazing

2.1 Conditional Assumptions

The various assumed conditions are as follows: (1) The laser beam remains unaffected by boundary conditions, possessing a uniform power distribution, stable focus, and collimation. (2) The wetting capability of the filler material post-melting and its material's isotropy are disregarded. (3) Any possible phase changes in the materials during the welding process, such as solid-to-liquid melting, are neglected. (4) It is assumed that the contact between the weld and the base material during the welding process is perfectly sound, with no gaps or air layers. (5) The model in the paper is based on an ambient temperature of 20℃, convective heat transfer coefficient of 20J/m^2/s/℃, and radiative heat transfer coefficient of 0.85.

2.2 Mathematical Modelling

The numerical analysis of the temperature field in laser wire-fill brazing of copper-aluminum heterogeneous metal materials represents a typical nonlinear transient heat conduction problem. Some material characteristics undergo significant changes due to variations in ambient temperature. Therefore, in numerical simulations, Fourier analysis is commonly employed to investigate nonlinear and non-equilibrium phenomena. The nonlinear three-dimensional transient heat conduction function is characterized by the following heat transfer partial differential equation [16-18]:

$$\rho \mathrm{c}\frac{\partial \mathrm{T}}{\partial \mathrm{t}}-\frac{\partial}{\partial x}(k_x\frac{\partial T}{\partial x})-\frac{\partial}{\partial y}(k_x\frac{\partial T}{\partial y})-\frac{\partial}{\partial z}(k_x\frac{\partial T}{\partial z})=Q(x,y,z,t)+H \qquad (1)$$

in the equation, T represents temperature; t denotes time; ρ signifies density; k stands for thermal conductivity coefficient; c corresponds to specific heat capacity; Q denotes the magnitude of heat source intensity; and H represents latent heat.

For molten metallic materials, these are considered incompressible fluids, and in the simulation process, the flow of the metal is assumed to be laminar. For the three-dimensional problem of incompressible fluids, when assuming constant pressure, specific heat capacity, and thermal conductivity coefficient, the basic form is as described below [19].

The equation of mass conservation is given by:

$$\frac{\partial \mathrm{u}}{\partial \mathrm{x}}+\frac{\partial \mathrm{v}}{\partial \mathrm{y}}+\frac{\partial \mathrm{w}}{\partial \mathrm{z}}=0 \tag{2}$$

where u, v, and w represent the velocity components in the three orthogonal directions of the coordinate system.

The energy conservation equation is given by:

$$\rho C_{\mathrm{p}}\left(\frac{\partial T}{\partial \mathrm{t}}+\mathrm{u}\frac{\partial T}{\partial \mathrm{x}}+\mathrm{v}\frac{\partial T}{\partial \mathrm{y}}+\mathrm{w}\frac{\partial T}{\partial \mathrm{z}}\right)=\frac{\partial}{\partial \mathrm{x}}\left(\mathrm{k}\frac{\partial \mathrm{T}}{\partial \mathrm{x}}\right)+\frac{\partial}{\partial \mathrm{y}}\left(\mathrm{k}\frac{\partial \mathrm{T}}{\partial \mathrm{y}}\right)+\frac{\partial}{\partial \mathrm{z}}\left(\mathrm{k}\frac{\partial \mathrm{T}}{\partial \mathrm{z}}\right)+\mathrm{S}_{H} \tag{3}$$

where, T represents temperature; ρ is density; C_p stands for specific heat capacity at constant pressure for the fluid; k denotes thermal conductivity; S_H represents the source term of the energy equation.

The equation of momentum conservation is:

In the x-direction:

$$\rho\left(\frac{\partial \mathrm{u}}{\partial \mathrm{t}}+\mathrm{u}\frac{\partial \mathrm{u}}{\partial \mathrm{x}}+\mathrm{v}\frac{\partial \mathrm{u}}{\partial \mathrm{y}}+\mathrm{w}\frac{\partial \mathrm{u}}{\partial \mathrm{z}}\right)=-\frac{\partial \mathrm{P}}{\partial \mathrm{x}}+\mu\left(\frac{\partial^{2}\mathrm{u}}{\partial \mathrm{x}^{2}}+\frac{\partial^{2}\mathrm{u}}{\partial \mathrm{y}^{2}}+\frac{\partial^{2}\mathrm{u}}{\partial \mathrm{z}^{2}}\right)+\mathrm{F}_{\mathrm{x}} \tag{4}$$

In the y-direction:

$$\rho\left(\frac{\partial \mathrm{v}}{\partial \mathrm{t}}+\mathrm{u}\frac{\partial \mathrm{v}}{\partial \mathrm{x}}+\mathrm{v}\frac{\partial \mathrm{v}}{\partial \mathrm{y}}+\mathrm{w}\frac{\partial \mathrm{v}}{\partial \mathrm{z}}\right)=-\frac{\partial \mathrm{P}}{\partial \mathrm{y}}+\mu\left(\frac{\partial^{2}\mathrm{v}}{\partial \mathrm{x}^{2}}+\frac{\partial^{2}\mathrm{v}}{\partial \mathrm{y}^{2}}+\frac{\partial^{2}\mathrm{v}}{\partial \mathrm{z}^{2}}\right)+\mathrm{F}_{\mathrm{y}} \tag{5}$$

In the z-direction:

$$\rho\left(\frac{\partial \mathrm{w}}{\partial \mathrm{t}}+\mathrm{u}\frac{\partial \mathrm{w}}{\partial \mathrm{x}}+\mathrm{v}\frac{\partial \mathrm{w}}{\partial \mathrm{y}}+\mathrm{w}\frac{\partial \mathrm{w}}{\partial \mathrm{z}}\right)=-\frac{\partial \mathrm{P}}{\partial \mathrm{z}}+\mu\left(\frac{\partial^{2}\mathrm{w}}{\partial \mathrm{x}^{2}}+\frac{\partial^{2}\mathrm{w}}{\partial \mathrm{y}^{2}}+\frac{\partial^{2}\mathrm{w}}{\partial \mathrm{z}^{2}}\right)+\mathrm{F}_{\mathrm{z}} \tag{6}$$

Where μ is the dynamic viscosity of the fluid; P represents pressure; F_x, F_y, F_z denote the source terms of the momentum equations in the three Cartesian coordinate directions.

2.3 Thermal Source Model

The thermal source on the laser follows a Gaussian distribution, as depicted in Fig 1. Its functional expression is given by:

$$q=\frac{aP}{\pi R^{2}}\exp\left[-\left(\frac{ar^{2}}{R^{2}}\right)\right] \tag{7}$$

$$q(r)=\frac{6\sqrt{3}f_1}{\pi^{3/2}abc_f}\exp(-3(\ (\frac{x}{a})^2+(\frac{y}{b})^2+(\frac{z}{c_f})^2)\ ),\ y\geq 0 \quad (8)$$

$$q(r)=\frac{6\sqrt{3}f_2}{p^{3/2}abc_r}\exp(-3(\ (\frac{x}{a})^2+(\frac{y}{b})^2+(\frac{z}{c_r})^2)\ ),\ y\geq 0 \quad (9)$$

Where x, y, z are the coordinate values; a, b, c are shape parameters of the heat source corresponding to the semi-axes of the laser ellipsoidal heat source; a represents the concentration coefficient of the heat flux; P stands for effective power; c_f, c_r are the lengths of the front and back halves of the ellipsoid, respectively.

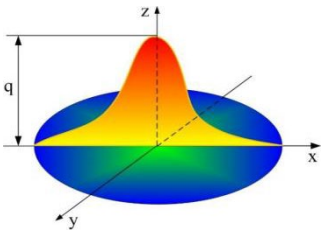

Fig. 1. Gaussian Heat Source Distribution

Assuming the internal energy within the small aperture follows a Gaussian cylindrical heat source and is uniformly distributed along the vertical direction, the volumetric heat source can be represented as follows:

$$q(r,z)=\frac{2P}{\pi r_0^{\ 2}h}\exp(-\frac{2r^2}{r_0^{\ 2}}) \quad (10)$$

In this equation, r_0 represents the effective radius of the heat source, and for calculations, we take r_0=R/2; h is the thickness of the specimen, R is the characteristic radius of the heat flow distribution, P stands for effective power, r is the distance from any point on the surface of the welded specimen to the centre of the light source.

2.4 Material Physical Properties

In this study, T2 copper and aluminum alloy 6063 were selected as the materials for the curved plates, and $CuSi_3$ welding wire was chosen for brazing. The left side represented copper, and the right side represented aluminum alloy in the welding process (see Fig 2). The physical properties of these materials change with temperature variations. To address convective heat transfer involving latent heat and molten pool convection, the effective heat fusion method [20-22] and thermal conductivity correction [23] were employed in the numerical simulation experiments.

This article selects T2 copper and aluminum alloy 6063 as heterogeneous alloy materials, and the thermal conductivity and specific heat of the two materials vary with temperature as shown in Figures 3 and 4. $CuSi_3$ welding wire was selected

as the brazing material for two heterogeneous alloys, and the specific material parameters are shown in Figure 5. It can be seen that the thermal conductivity of the T2 Copper material increases significantly with increasing temperature, while the specific heat capacity has the opposite trend. The specific heat capacity of Aluminum Alloy 6063 increases with increasing temperature, while its thermal conductivity remains almost unchanged. The thermal conductivity and specific heat capacity of the CuSi3 solder both increase with increasing temperature and show good thermal stability.

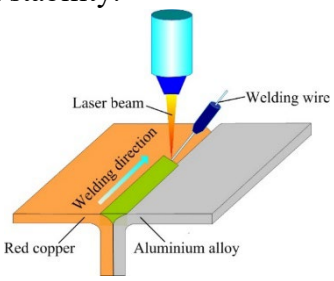

Fig. 2. Illustration of Laser Wire-Fill Brazing

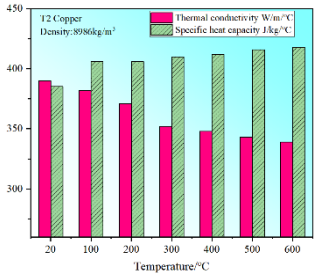

Fig. 3. Physical Properties of T2 Copper

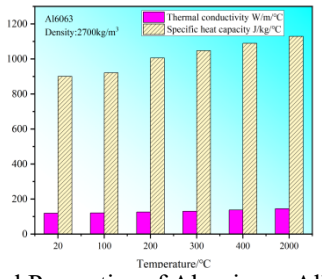

Fig. 4. Physical Properties of Aluminum Alloy 6063

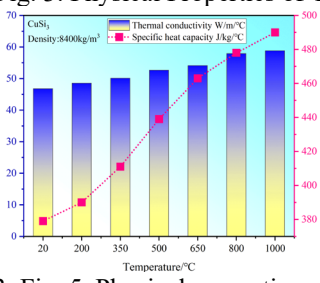

Fig. 5. Physical properties of $CuSi_3$ solder

2.5 Finite Element Model and Mesh Generation

In the finite element model of laser-assisted brazing, the welding area is divided into the fusion, boundary, and heat-affected zones. Precise dimensions of 100mm×32mm×1mm were chosen for the metal plate, and a 100mm length of CuSi3 brazing wire was used. The brazing wire mesh was finer to ensure accuracy. The model, as shown in Fig 6, employed birth and death elements to simulate the melting and cooling of the brazing material during the welding process. This was realized through specialized subroutines.

Fig. 6. Mesh division

2.6 Model validation

In order to verify the reliability of the model, a welding experiment between T2 purple copper and aluminum alloy 6063 was established. In the experiment, the size is 100mm × 32mm × 1mm T2 purple copper plate with a size of 100mm × 100mm × 1mm aluminum alloy 6063 plate was welded, the CuSi3 welding wire was used as brazing material, and welding robots were used for welding. During the welding process, temperature measurement equipment was used to monitor the temperature in real time, as shown in Fig. 7(a). Meanwhile, the same numerical analysis model was established using the modeling method proposed in this paper, and the temperature observations of the specimen reference points were extracted. Finally, the experimental data were compared with the results of the numerical analysis model, and the temperature change curve shown in Fig. 7(b) was obtained.

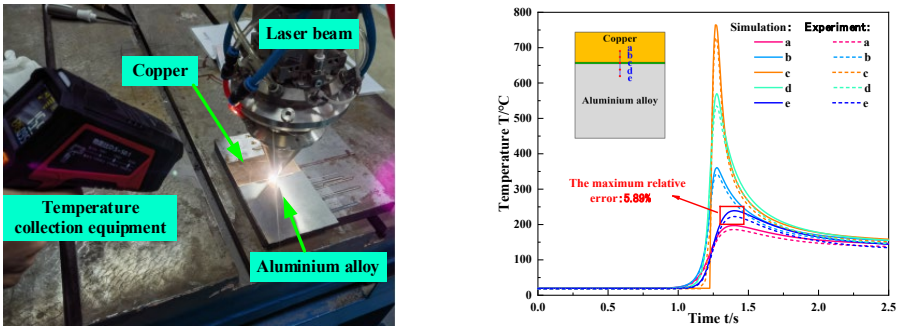

(a) Experimental equipment and process (b) Temperature variation curve

Fig. 7 Temperature measurement experiment for welding

According to the data in Fig. 7(b), it can be seen that the temperature values measured by the experiment are all slightly lower than the calculated values, which is mainly due to the lower temperature of the experimental environment, which accelerates the heat dissipation of the welding process. The temperature trends obtained from the experiment and simulation calculation are consistent with each other, and the maximum relative error is only 5.89%, which verifies the correctness of the model.

3 Simulation Results and Numerical Analysis

3.1 Analysis of Welding Temperature Field

By employing numerical simulation, this study analyzed the variations in temperature fields during the laser wire feeding brazing process. The laser output power was set at approximately 1.1 kW, while the welding speed was maintained at around 0.04 m/s. The entire process lasted for approximately 2.5 seconds. Subroutines were utilized to achieve these specific parameters. During the welding

process, a numerical simulation was conducted using the method of finite element analysis to study the formation of the weld seam. In this approach, units that were not involved in the welding process were treated as inactive units and were not considered in the heat conduction calculations. However, due to the heating from the laser heat source, as the welding progressed, these inactive units were sequentially activated to simulate the entire wire feeding welding process. Eventually, the brazing material melted and filled the joint, resulting in a complete weld seam.

A temperature distribution contour plot during the welding process is shown in Fig 8. As depicted in the figure, during laser brazing, the high-temperature welding radiation zone forms an elliptical shape, which differs from the localized high-temperature spots typically observed in conventional laser melting welding.

Fig 9 showcases transient temperature field distributions at various time instances during the welding process. It depicts the dynamic thermal profiles of the welded components, precisely captured at time intervals of 0.5s, 1.25s, 2.0s, and 2.5s. Furthermore, a designated pathway is established at a distance of 19mm from the initiation point of welding, as illustrated in Fig 10. At specific time points, namely t=0.5s, t=1.25s, t=2.0s, and t=2.5s, the temperature variations at each node along the pathway are meticulously recorded, as presented in Fig 11. This meticulous examination endeavors to unravel the intricate nuances of temperature fluctuations within the plate material.

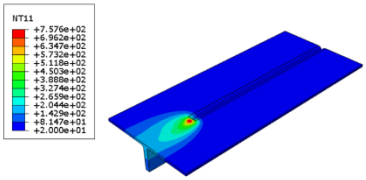

Fig. 8. Temperature distribution map

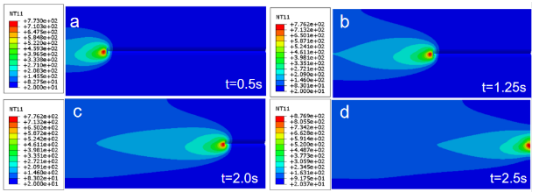

Fig. 9. Transient temperature field maps at different time intervals

Fig. 10. Illustration of path node diagram

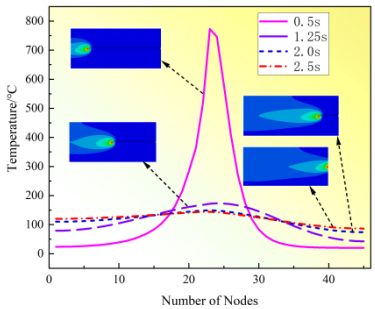

Fig. 11. Thermal cycling curves at different time points along the path

From the illustration, it becomes apparent that the temperature field in the laser-based brazing process of copper-aluminum heterogeneous metals exhibits an

asymmetric distribution on either side of the weld gap. Notably, the temperature field distribution on the copper side surpasses that of the aluminum side. This discrepancy arises from the divergent thermal conductivity and specific heat between the two dissimilar metallic materials at varying temperature levels. Specifically, copper exhibits a greater heat conductivity compared to aluminum.

Around 0.5 seconds into the heating process, the temperature contour lines appear more dispersed, indicating an expansion in the effective range of the heat source due to elevated temperatures. During this period, the welding plate absorbs heat, leading to a widening and gradual broadening of the heating device's influence zone.

At 1.25 seconds and 2.0 seconds, the temperature distribution plots within the welding area (as shown in Fig 9(b) and (c)) demonstrate a rapid temperature change in the front region of the laser heat source. This phenomenon can be attributed to the laser heat source's high energy density, which instantaneously heats the welding area, resulting in a rapid temperature increase and the formation of temperature gradients. Similarly, the temperature contour lines in the region behind the heat source exhibit an approximately circular trend, while in the areas further away from the heat source, the temperature contour lines take on an elliptical shape and elongate in the direction of the weld.

At 2.5 seconds, the influence of the highest temperature extends to its maximum extent on the edge region of the lap joint. This situation may potentially lead to the occurrence of weld penetration in the steel plate.

3.2 Thermal cycle curve in welding process

In order to explore the thermal cycle curve in the welding process, four points are evenly selected in the welding direction of the center line of the brazing seam during welding. The distance of each node is 25mm, and Figure 12 shows the thermal cycle curve of the selected node. As can be seen from the figure, the temperature of the laser heat source is low at the beginning of welding. With the movement of the laser heat source, the weldment absorbs heat and the temperature rises. And the temperature of the area directly acted by the laser heat source rises sharply, and the temperature of the area after the corresponding laser heat source passes decreases. At the end of welding, there will be a sudden change in the highest temperature at this point. This is due to at the terminal of welding, no material at the end of welding metal material absorbs heat, which leads to heat concentration at the end of welding metal material, therefore, the temperature at this point is the highest.

For deeply study the change of temperature field in the process of laser brazing with wire filler, five points are selected in the direction perpendicular to the welding center line during welding. At the center of the brazing seam, four more

points are selected perpendicular to the welding direction to ensure the uniform distribution of the selected points, as shown in Figure 13, and defined as path 3. Among them, point c is the center point during welding, and points b and d are located in the vertical direction and 3mm away from point c (the edge position of the weld). While the centers of point a and point e are located in the vertical direction and 6mm away from point c.

Point a is on the copper plate, point e is on the aluminum alloy plate, point b is on the weld edge of the copper alloy plate, and point d is on the weld edge of the aluminum plate. As shown in fig. 14, the highest temperatures at points a and b are lower than those at points d and e. This is due to aluminum alloy has a large specific heat capacity, which can absorb more heat and the temperature rises higher, but copper alloy has a small specific heat capacity and absorbs relatively less heat.

Due to the heterogeneity of copper and aluminum materials, their thermodynamic properties are different, which leads to different temperature changes on the left and right sides of the joint. In order to explore the variation law of temperature related to heterogeneous metals in more detail, a path is established at the distance of 4mm from the weld center on both sides of copper and aluminum, which is defined as path 4.

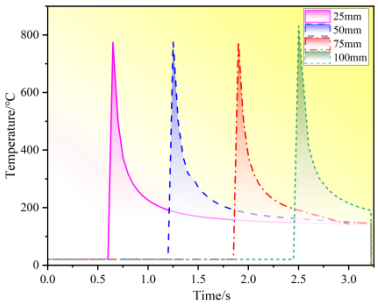

Fig. 12. Thermal cycle curves at different points on path 2

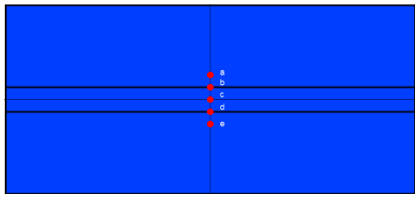

Fig. 13. Schematic diagram of path 3

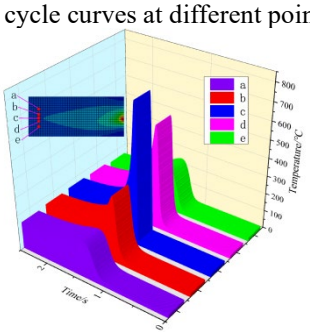

Fig. 14. Thermal cycle curve corresponding to path 3

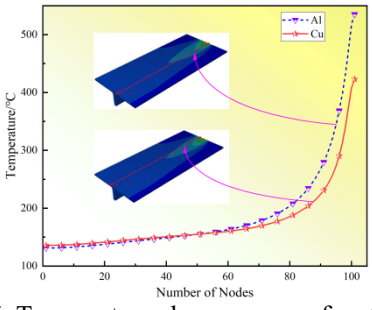

Fig. 15. Temperature change curve of metal plates on both sides along path 4

As shown in fig. 15, due to the high thermal conductivity of copper alloy, it can conduct heat from the welding area to the area far away from the welding area

more quickly. Therefore, the temperature of copper alloy plate far away from welding is relatively high. On the other side, aluminum alloy has a higher specific heat capacity and requires more heat to raise its temperature. In the welding process, the aluminum alloy plate close to the welding place can absorb more heat, resulting in higher temperature.

3.3 Influence of laser power on temperature field in welding process

Laser power is one of the vital parameters in laser welding, which has great influence on welding quality. Fig. 16 is a nephogram showing the distribution of the transient temperature field when the welding speed is 0.04m/s and the laser output power is 900W, 1,000 W, 1,100 W, 1,300 W and 1,500 W respectively (t=1.25s). As can be seen from the figure, with the increase of laser power, the energy input of the laser beam increases correspondingly, thereby strengthening the heat transfer effect during the welding process. This phenomenon leads to more heat concentration in the welding area, further expanding the heat affected zone.

According to the results in fig. 16, when the laser power is 1100W, the heat affected zone reaches a suitable range. At this power, the welding area can be fully heated and complete the required melting and diffusion process. Meanwhile, the size of the heat affected zone is also moderate, which will not cause excessive temperature gradient and adverse effects.

To explore the optimal welding power, select a path on the centerline of the weld seam after welding, as shown in Figure 17, to study the temperature changes after welding.

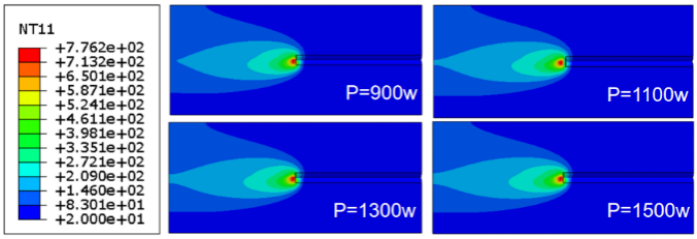

Fig. 16. Distribution nephogram of transient temperature field under different laser power

It can be seen from fig. 18 that with the increase of laser power, the highest temperature during welding also increases. When the laser power is 1100w, the highest temperature is about 800℃, which can fully melt the solder without exceeding the melting point of copper alloy. However, at lower laser power, the solder may not be fully melted, resulting in a decline in welding quality. On the contrary, when the laser power is too high, the welding temperature gradient span will become very large. It will lead to a sharp rise in the temperature during welding, even the phenomenon of welding penetration, and will affect the strength and stability of welded joints.

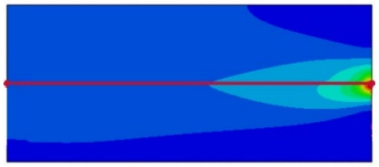

Fig. 17. Selection diagram of path 5

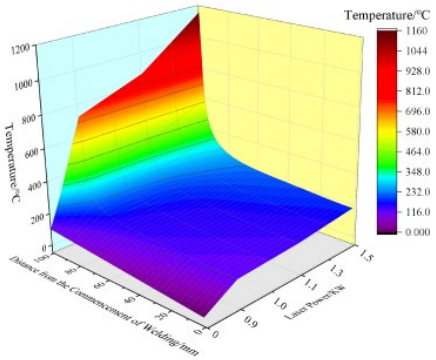

Fig. 18. Temperature change curve on welding center line after welding with different laser power

3.4 Influence of welding speed on temperature field in welding process

Welding speed is an important parameter in the process of laser wire-filled brazing, which has a direct impact on the quality and performance of welded joints. Fig. 19 is a nephogram of temperature field distribution when welding laser power P=1100w and welding speed are 0.01m/s, 0.02m/s, 0.04m/s and 0.08m/s respectively (t=1.0s). From the figure, it can be seen that the heat affected zone during welding increases with the decrease of welding speed, and the diameter of the light spot decreases with the increase of welding speed. When the welding speed is low, the heat input will increase, and more heat will be transferred to the base metal during welding, which will lead to the expansion of the heat affected zone. This is due to when the welding speed is slow, the heat has more time to spread to the surrounding area through conduction and diversion, thus increasing the thermal influence range. When the welding speed is fast, the corresponding phenomenon is the opposite. Due to insufficient time for heat to diffuse to the surrounding area, the range of heat impact is relatively small.

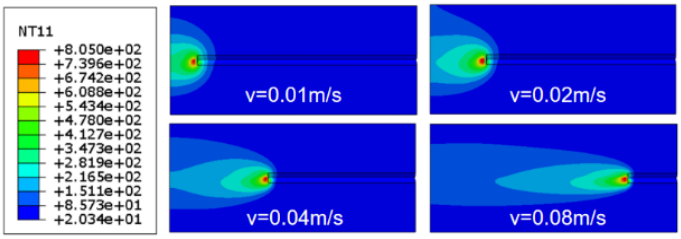

Fig. 19. Nephogram of temperature field with different speeds at the same time

The optimal welding speed range is studied through the temperature field distribution of molten pool produced in the welding process. At four welding speeds, the nephogram of cross-section temperature field when welding is in the middle position of the plate is selected respectively, as shown in Figure 20. And extract the temperature curve at the cross section of two plates, as shown in Figure

21. From the figure, it can be seen that due to the different materials of the two metal plates during welding, the temperature field distribution of the molten pool during welding is asymmetric.

When the welding speed is 0.01m/s or 0.02m/s, due to the slower welding speed, the plate absorbs more heat. This will lead to a large molten pool volume and an enlarged high temperature area during welding. When the welding speed is 0.08m/s, due to the high welding speed, the temperature distribution of the entire molten pool is not uniform enough. This will lead to incomplete melting of solder or incomplete combination with base metal, which will affect the welding quality. When the welding speed is 0.04m/s, the temperature field distribution of the molten pool is relatively uniform, and the highest temperature is in a relatively stable position. These can not only make the solder melt stably, but also ensure the full integration of the solder and the base metal.

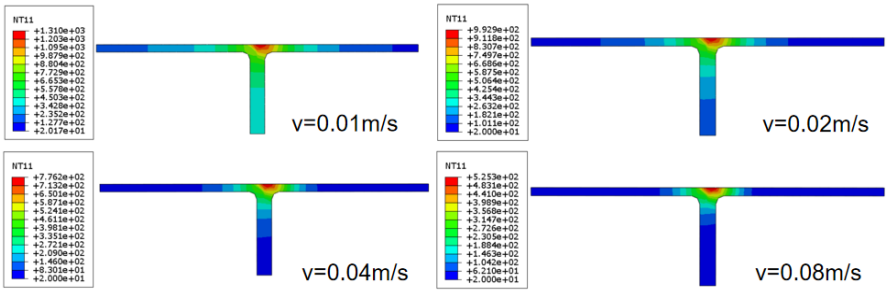

Fig. 20. Temperature field distribution of weldment section under different welding speeds

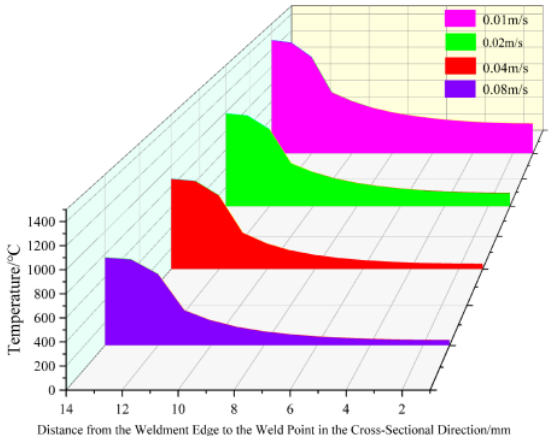

Fig. 21. Thermal cycle curves of weldments at different welding speeds

4 Conclusions

Based on the nonlinear transient heat conduction theory, a mathematical model of laser wire-filled brazing is established in this paper. Through finite element numerical simulation, the temperature field data extracted after various factors change are analyzed, and the following conclusions are drawn:

(1) During laser brazing of Cu-Al heterogeneous alloy materials, it was found that the temperature on the copper alloy side was obviously higher than that on the aluminum alloy side, and the temperature field of the metal plates on both sides showed asymmetric distribution. The high temperature welding temperature field formed by laser is an elliptical shape with temperature gradient change. With the increase of welding time, the isotherm in the welding area began to become sparse and elongated along the weld direction.

(2) It is found that laser power has great influence on welding quality. With the increase of laser power, the maximum temperature of welding will also increase, but too high power will lead to weld width and even weld penetration. When the laser power is too low, the solder can not be fully melted, and the phenomenon of incomplete penetration will occur.

(3) With the increase of welding speed, the maximum welding temperature decreases, the spot diameter decreases and the weld pool width narrows, which is a benign effect. However, if the welding speed is too high, the quality of the welded joint will be uneven, and if the welding speed is too low, the temperature will be too high, and welding penetration may occur.

(4) Through comparative study, it is found that when the laser power is P=1100w and the welding speed is 0.04m/s, the highest temperature is about 800℃, which can fully melt the solder without exceeding the melting point of copper alloy, and high-quality welded joints can be obtained, thus optimizing the brazing process.

Funding:

The author(s) disclosed receipt of the following financial support for the research, authorship, and/or publication of this article: Henan Province Science and Technology Research Project (No.222102240017, 212102110023), for their support to this research.

REFERENCES

[1]. *Yiyang Hu*, *Yiming Zhang*, *Gaoyang Mi*, et al. Effects of Si contents in filling wires on microstructure evolution and properties of Al-steel dissimilar joint by laser welding-brazing. Journal of Materials Research and Technology, 2021, (15): 1896-1904.

[2]. *Yan Li*, *Dezhi Yang*, *Wenyu Yang*, et al. Multiphysics numerical simulation of the transient forming mechanism of magnetic pulse welding. Metals, 2022, 12(7): 1149.

[3]. *Yajie Li*, *Fengming Qin*, *Zhisheng Wu*. Flow Patterns, Microstructure and Mechanical Properties of AZ31/Al6061 Dissimilar Friction Stir-Welded Joints. Journal of Materials Engineering and Performance, 2019, 28(9).
[4]. *Wallerstein, Daniel,* et al. Advanced characterization of intermetallic compounds in dissimilar aluminum-steel joints obtained by laser welding-brazing with Al Si filler metals. Materials Characterization 179(2021):111345.
[5]. *Chioibaşu, Diana*, *Călin, Bogdan*, *Popescu, Andrei*, et al. Optimization of Laser Butt Welding of Stainless Steel 316l Using Response Surface Methodology, UPB Scientific Bulletin, Series A: Applied Mathematics and Physics, 2020, 82(2): 221-230.
[6]. *Zhang, Dengkui*, et al. Microstructure and Mechanical Properties of 2219 Aluminum Alloy/T2 Copper Explosively Welded Composite Plate. Journal of Materials Engineering and Performance, 2022, 31(12): 9681-9689.
[7]. *Shen Zhigang*, *Wu Zhisheng*, *Wang Ting*, et al. Research on Technology of 7075 Aluminum Alloy Processed by Variable Polarity TIG Additive Manufacturing Utilizing Nanoparticle-Reinforced Welding Wire with TiB2. Crystals, 2022, 12(12):1801.
[8]. Song Gang, Yu Jingwei, Li Taotao, et al. Effect of laser-GTAW hybrid welding heat input on the performance of Mg/Steel butt joint. Journal of Manufacturing Processes. 2018,31:131-138.
[9]. *Yiyang Hu*, *Zhang Yiming*, *Gaoyang Mi*, et al. Effects of Si contents in filling wires on microstructure evolution and properties of Al-steel dissimilar joint by laser welding-brazing. Journal of Materials Research and Technology, 2021,15: 1896-1904.
[10]. *Wan Xiulian*, *Wang Long*, *Yao Zhiwen* et al. Laser Filling Brazing Technology of Aluminum/Copper Dissimilar Metals. Chinese Journal of Rare Metals, 2019, 43(5):494-499.
[11]. *Dimatteo V*, *Ascari A*, *Liverani E*, et al. Experimental investigation on the effect of spot diameter on continuous-wave laser welding of copper and aluminum thin sheets for battery manufacturing. Optics and laser technology, 2022,145:107495-.
[12]. *Envelope KMA*, *PP A*. Artificial neural network to predict the weld status in laser welding of copper to aluminum. Procedia CIRP, 2021,103:61-66.
[13]. J*iankang Huang*, *Tao Yang*, *Xiaoquan Yu*, et al. Study of Interfacial Microstructure and Phase Evolution of Al/Cu Arc Welding-brazing Joint. Chinese Journal of Mechanical Engineering, 2020, 56(6):17-23.
[14] *Jin Yuhua*, et al. Effect of Post-Weld Annealing on Microstructure and Growth Behavior of Copper/Aluminum Friction Stir Welded Joint. Materials, 2020,20(13):4591.
[15]. *Kaisheva Darina*, *Anchev Angel*, *Dunchev*, Vladimir Electron-Beam Welding Cu and Al6082T6 Aluminum Alloys with Circular Beam Oscillations. Crystals, 2022,12(12):1757.
[16]. *Chang Wang*, *Zhongfeng Zhou*. Numerical simulation study on temperature field of laser filler wire brazing. Laser and Infrared. 2021,51(06):742-746.
[17]. Farid Vakili-Tahami, Peyman Majnoun, Navid Akhlaghifar. Numerical Simulation of the T-Shape Filletwelds of 304 and 1020 Steel Plates, UPB Scientific Bulletin, Series D: Mechanical Engineering, 2017, 79(2): 103-118.
[18]. Sabah Khammass Hussein. Analysis of The Temperature Distribution Infriction Stir Welding of AA 2024-T3 and AA6061-T6 Using Finite Element Method, UPB Scientific Bulletin, Series D: Mechanical Engineering, 2016, 78(4): 119-132.
[19]. *Xiaosong Feng*. Study on Laser Brazing with Filler Wire for Galvanized Steel Sheets and Numerical Simulation of the Thermal Process. Harbin Institute of Technology, 2007:72-75.
[20]. *Jian Qiao*, *Peng Yu*, *Yanxion Wu*. A Compact Review of Laser Welding Technologies for Amorphous Alloys.2020,12(10),1690.
[21]. *Yang*, *Fan,* et al. Research progress of laser welding under subatmospheric pressure. The International Journal of Advanced Manufacturing Technology 116 (2021): 803-820.

[22]. *Wang J*, *Fu X*, *Zhang L*, et al. A short review on laser welding/brazing of aluminum alloy to steel. The International Journal of Advanced Manufacturing Technology, 2021, 112: 2399-2411.
[23]. *Jing Li*, *Yanhui Feng*, *Xinxin Zhang*, et al. Thermal conductivity correction of metal nanowires considering interface scattering. Acta Physica Sinica, 2013,62(18):390－397.